Discrimination Ability Analysis on Texture Features for Automatic Noise Reduction in Brain MR Images

Yu-Ning Chang and Herng-Hua Chang*

Computational Biomedical Engineering Laboratory (CBEL) Department of Engineering Science and Ocean Engineering National Taiwan University, Daan, Taipei 10617, Taiwan

Abstract: Noise is one of the main sources of quality deterioration not only for visual inspection but also in computerized processing in magnetic resonance (MR) image analysis such as tissue classification, segmentation and registration. Accordingly, noise removal in brain MR images is important for a wide variety of subsequent processing applications. Most existing denoising algorithms require laborious tuning of parameters that are often sensitive to specific image features and textures. Automation of these parameters through artificial intelligence techniques will be highly beneficial. This paper attempts to systematically investigate significant attributes from popular image features and textures to facilitate subsequent automation process. In our approach, a total number of 39 image attributes are considered that are based on three categories: 1) Image statistics. 2) Gray-level co-occurrence matrix (GLCM). 3) Tamura texture features. To obtain the ranking of discrimination in these texture features, a T-test is applied to each individual image features computed in every image based on noise levels, intensity distributions, and anatomical geometries. Preliminary results indicated that the order of significance in the texture features approximately varies in noise, slice, and normality. For distinguishing between noise levels, the features of contrast, standard deviation, angular second moment, and entropy from the GLCM class performed best. For distinguishing between slice positions, the features of mean and variance from the basic statistics class and the coarseness feature from the Tamuraclass outperformed other features.

Keywords: MRI, Image feature, Image texture, Noise reduction.

1. INTRODUCTION

Neuroimaging is one powerful tool used to investigate the structure and function of the brain in both health and disease [1]. Magnetic resonance imaging (MRI) has been one of the most frequently used neuroimaging modalities due to its high contrast among different soft tissues, high spatial resolution across the entire field of view, and multi-spectral characteristics [2, 3]. The functional MRI (fMRI) is a functional neuroimaging procedure that uses MRI technology to measure brain activity by detecting associated changes in blood flow. Recently, diffusion anisotropy measures derived from diffusion tensor MRI (DT-MRI) data, such as fractional anisotropy, relative anisotropy and ellipsoidal area ratio, are commonly used to assess microstructural features and white matter connectivity in the human brain. In particular, the diffusion-weighted images (DWIs) are used to estimate diffusion tensors and their derivative measures of anisotropy.

However, random noise usually appears during the acquisition of all described MR images above that includes eddy-current distortions, physiological motion and instabilities of the MRI scanning hardware [4, 5]. The noise not only affects the medical diagnostic tasks but also degrades many computerized image processing and analysis procedures such as tissue classification, visualization, super-resolution, segmentation, and registration. For example, the influences of noise in DWI data can impair the validity and precision of tensor estimation. Consequently, noise removal or reduction is important and essential to maintain the quality of brain MR images for a wide variety of subsequent applications.

Nevertheless, most denoising algorithms require laborious tuning of parameters that are often sensitive to specific image features and textures [6-10]. Automation of these parameters through artificial intelligence techniques will be highly beneficial. However, this will induce another problem of seeking appropriate meaningful attributes among a huge number of image characteristics for the automation process. This paper attempts to systematically investigate significant attributes from widely used image features and textures for future developments in the automation process.

2. METHODS

The proposed scheme consists of two phases: feature extraction and feature selection, as illustrated in Figure **1**.

*Address correspondence to this author at the Department of Engineering Science and Ocean Engineering National Taiwan University 1 Sec. 4 Roosevelt Road, Daan, Taipei 10617, Taiwan; Tel: +886-2-3366-5745; Fax: +886-2-2392-9885; E-mail: herbertchang@ntu.edu.tw

E-ISSN: 2409-3394/15

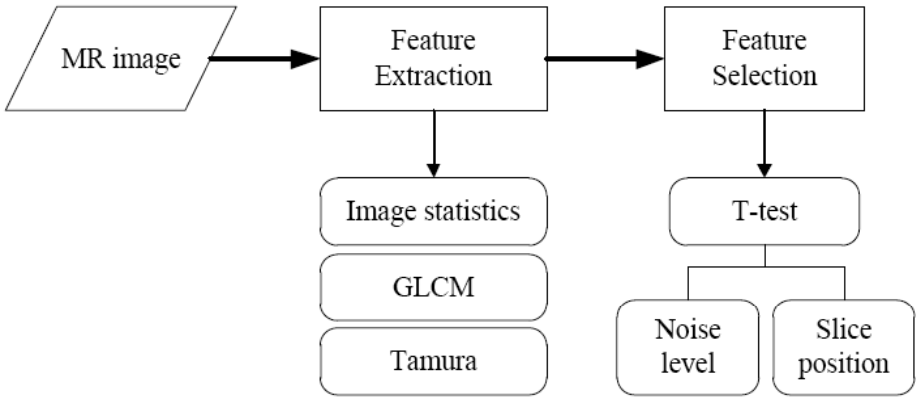

Figure 1: Flow chart of the proposed schemes to investigate the discrimination ability of texture features extracted from three different categories: basic image statistics, gray level co-occurrence matrix (GLCM) and Tamura texture feature.

2.1. Texture Feature Extraction

There are 39 different image features that are obtained based on the three different feature extraction categories in every single image as following.

2.1.1. Basic Image Statistics

We compute the mean intensity (Mean), standard deviation (SD), variance (VAR), and entropy (ENT) of the input gray-level image.

2.1.2. Gray Level Co-occurrence Matrix (GLCM)

The gray level co-occurrence matrix (GLCM)[11] describes some easily computable textural features based on gray tone spatial dependencies using

$$M(i,j) = \sum_{x=1}^{W_x-\Delta x} \sum_{y=1}^{W_y-\Delta y} \begin{cases} 1, \text{if } W(x,y) = i \text{ and } W(x+\Delta x, y+\Delta y) = j \\ 0, \text{otherwise} \end{cases} \quad (1)$$

Where $M(i,j)$ is the quantized gray tone at position (i,j), W_x and W_y are the dimension of the resolution cells of the image ordered by their row-column designations, $W(x,y)$ is the gray level value in the cell, Δx and Δy are the spatial relation between two adjacent pixels defined by the angle θ and distance d from the cell origin. This texture-content information is then normalized to obtain the matrix of relative frequencies $P(i,j)$ as

$$P(i,j) = \frac{M(i,j)}{\sum_{i=0}^{W_x-1} \sum_{j=0}^{W_y-1} M(i,j)} \quad (2)$$

Table **1** summarizes the textural features based on Eq. (2). We first compute the difference image I_n, which is the difference between the input image *I* and its Gaussian filtered image I_D based on Eq. (3). Compute the textural features of GLCM using I_n with d = 1.

$$I_n = I - I_D \quad (3)$$

2.1.3. Tamura Texture Features

Tamura texture features [12-14] are calculated based on human visual and psychological perception, and We compute three Tamura features, namely, coarseness (COA), contrast (CON), directionality (DIR) of the input gray-level image. The three features are correlated closely with human perception and can be measured by the following

a). Coarseness

Take the average intensity value at every pixel (x,y) over neighborhoods whose sizes are integer powers of 2:

$$A_k(x,y) = \frac{1}{2^{2k}} \sum_{i=x-2^{k-1}}^{x+2^{k-1}-1} \sum_{j=y-2^{k-1}}^{y+2^{k-1}-1} f(i,j) \quad (4)$$

where $f(i,j)$ is the gray level at (i,j), $k \in \langle 0,.....,5 \rangle$

For each pixel (x, y) take the differences between pairs of averages of non-overlapping neighborhoods on the opposite side of the point in both horizontal and vertical directions as

Horizontal Case

$$E_{k,h}(x,y) = |A_k(x+2^{k-1},y) - A_k(x-2^{k-1},y)| \quad (5a)$$

Vertical Case

$$E_{k,v}(x,y) = |A_k(x,y+2^{k-1}) - A_k(x,y-2^{k-1})| \quad (5b)$$

Table 1: Textural Features and Equations of GLCM

Feature	Equation
Angular Second Moment	$ASM = \sum_{i=0}^{M-1}\sum_{j=0}^{M-1} P_{ij}^2$
Contrast	$CON = \sum_{i=0}^{M-1}\sum_{j=0}^{M-1} P_{ij}(i-j)^2$
Entropy	$ENT = \sum_{i=0}^{M-1}\sum_{j=0}^{M-1} P_{ij}(-lnP_{ij})$
Homogeneity	$HOM = \sum_{i=0}^{M-1}\sum_{j=0}^{M-1} \frac{P_{ij}}{1+(i-j)^2}$
Dissimilarity	$DIS = \sum_{i=0}^{M-1}\sum_{j=0}^{M-1} P_{ij}\lvert i-j\rvert$
Mean	$\mu_i = \sum_{i=0}^{M-1}\sum_{j=0}^{M-1} i(P_{ij}), \mu_j = \sum_{i=0}^{M-1}\sum_{j=0}^{M-1} j(P_{ij})$
Standard Deviation (SD)	$\sigma_i = \sqrt{\sum_{i=0}^{M-1}\sum_{j=0}^{M-1} P_{ij}(i-\mu_i)^2}\ \sigma_j = \sqrt{\sum_{i=0}^{M-1}\sum_{j=0}^{M-1} P_{ij}(j-\mu_j)^2}$
Correlation	$COR = \sum_{i=0}^{M-1}\sum_{j=0}^{M-1} P_{ij}\left[\frac{(i-\mu_i)(j-\mu_j)}{\sigma_i\sigma_j}\right]$

At each pixel, select the best size that gives $S_{best}(x,y) = 2^k$ the highest output value, where k maximizes *E* in either direction:

$$E_k(x,y) = \max\ \left(E_{k,h}(x,y), E_{k,v}(x,y)\right) \tag{6}$$

Finally, F_{crs} can be measured by:

$$F_{crs} = \frac{1}{M\times N}\sum_{i=1}^{M}\sum_{j=1}^{N} S_{best}(i,j) \tag{7}$$

Where M and N are the effective width and height of the image, respectively.

b). Contrast

$$F_{con} = \frac{\sigma}{\left(\frac{\sum_{i=1}^{M}\sum_{j=1}^{N}(f(i,j)-\mu)^4}{M\times N\times\sigma^4}\right)^n} \tag{8}$$

Where σ is the variance of the gray-level probability distribution, n is a positive number, and μ is the mean intensity.

Directionality

$$F_{dir} = 1 - r\times n_p \times \sum_{p}^{n_p}\sum_{\phi\in w_p}\left(\phi-\phi_p\right)^2 H_D(\phi) \tag{9}$$

$$|\Delta G| = \frac{|\Delta_H|+|\Delta_V|}{2} \tag{10}$$

$$\theta = \tan^{-1}\left(\frac{\Delta_V}{\Delta_H}\right) + \frac{\pi}{2} \tag{11}$$

where n_p is the number of peaks, $\varnothing_p$ is the p^{th} peak position of H_D, w_p is the range of the p^{th} peak between valleys, r is a normalizing factor related to quantizing levels of $\varnothing$, and H_D, is the edge probability histogram by quantizing θ using Eq. (11) and counting the points with the magnitude $|\Delta G|$ by Eq. (10) over a threshold t using

$$H_D(k) = \frac{N_\theta(k)}{\sum_{i=0}^{d-1} N_\theta(i)}, \mathrm{k} = 0, 1, \ldots, \mathrm{d}-1 \tag{12}$$

Where $N_\theta(k)$ is the number of points at which $(2k-1)\pi/2d \le \theta < (2k+1)\pi/2d$ and $|\Delta G| \ge t$. The purpose of thresholding $|\Delta G|$ by t is to prevent counting of unreliable directions, which are not regarded as edge points.

2.2. Feature Selection

To obtain the most significant attributes, a T-test [15, 16] is then applied to each individual image features to evaluate the ability of discrimination in two categories: *noise level* and *slice position*. The evaluation is based on the distinguishing ability between noise levels, intensity distributions, and anatomical geometries of two images according to the average *p*-value. The features with an average *p*-value<0.05 represent that they can effectively distinguish characteristics differences in image data [17].

3. EXPERIMENTAL RESULTS AND DISCUSSION

We used the famous Brain Web image data of normal and multiple sclerosis (MS) T1-weighted MR image volumes in five different thicknesses: 1mm, 3mm, 5mm, 7mm, and 9mm with various levels of noise and intensity non-uniformity to evaluate our methods[18].There were 4672 images in either anatomical type that resulted in 9344 images in total for the experiments. Tables **2** and **3** present the order of significance in the normal dataset based on the average p-value of each individual feature using the T-test for noise level and slice position, respectively. In Table **2**, for the case of the frequently used slice thickness of 1 mm, the contrast features in four directions in the GLCM class performed best, followed by the standard deviation features with respect to both axes in four directions. The best features for distinguishing between noise levels for the cases of 3 mm and 5 mm were the entropy and angular second moment in four directions in the GLCM class, respectively. While the standard deviation features played an important role in all slice thickness cases in Table **2**, the mean intensity feature had the best distinguishing ability between slice positions in Table **3**.The rankings of discrimination ability in the texture features for the MS cases in noise level and slice position are reported in Tables **4** and **5**, respectively. Once again, in Table **4**, the features of contrast, standard deviation, and entropy in the GLCM class outperformed other features in distinguishing between noise levels. In Table **5**, the mean intensity feature in the basic statistics class still performed best in distinguishing between slice positions.

Table 2: T-test Results of Normal Model Based on the P-Value: Noise Level

Thickness: 1mm	
p-value	Feature
<0.05	CON(0°, 45°, 90°, 135°), SD(x,0°, 45°, 90°, 135°), SD(y,0°, 45°, 90°, 135°),ASM(0°, 45°, 90°, 135°),HOM(45°),ENT(0°, 90°), DIS(90°, 135°), CON
< 0.1	COR(0°,45°,90°,135°),HOM(0°, 90°, 135°), ENT, SD,VAR,DIS(0°, 45°) ENT(135°,45°),
Thickness: 3mm	
p-value	Feature
<0.05	ENT(0°, 45°, 90°, 135°), CON(135°), ASM(0°), SD(x,0°, 45°, 90°, 135°), SD(y,0°, 45°, 90°, 135°), CON
< 0.1	CON(0°, 45°, 90°), DIS(0°, 45°, 90°, 135°), HOM(45°, 90°, 135°), COR(0°, 45°, 90°, 135°), ASM(45°, 90°, 135°)
Thickness: 5mm	
p-value	Feature
< 0.1	ASM(0°, 45°, 90°, 135°), SD(x,0°, 45°, 90°, 135°), SD(y,0°, 45°, 90°, 135°), DIS(0°, 45°, 90°, 135°), CON(0°, 45°, 90°, 135°), ENT(0°, 45°, 90°, 135°), COR(0°, 45°, 90°, 135°), HOM(45°, 135°), CON
Thickness: 7mm	
p-value	Feature
< 0.1	SD(x,0°, 45°, 90°, 135°),SD(y,0°, 45°, 90°, 135°), CON(0°, 45°, 90°, 135°), CON, HOM(45°, 135°), DIS(0°, 45°, 135°), ASM(0°, 45°, 90°, 135°), ENT(0°, 45°, 90°, 135°), COR(0°, 45°, 90°, 135°)
Thickness: 9mm	
p-value	Feature
< 0.1	SD(x,0°, 45°, 90°, 135°), SD(y,0°, 45°, 90°, 135°), CON(0°, 45°, 90°, 135°), ASM(0°, 45°, 90°), COR(0°, 45°, 90°), DIS(0°, 45°, 135°), HOM(45°, 135°), CON

Table 3: T-test Results of Normal Model Based on the P-Value: Slice Position

Thickness: 1mm, 3mm	
p-value	Feature
<0.05	Mean
< 0.1	COA
Thickness: 5mm, 7mm, 9mm	
p-value	Feature
<0.05	Mean
< 0.1	COA, VAR, SD

Table 5: T-test Results of Normal Model Based on the P-Value: Slice Position

Thickness: 1mm	
p-value	Feature
<0.05	Mean
< 0.1	COA
Thickness: 3mm	
p-value	Feature
<0.05	Mean, COA
Thickness: 5mm, 7mm, 9mm	
p-value	Feature
<0.05	Mean
< 0.1	COA, VAR, SD

4. CONCLUSION

We have investigated significant attributes from various image texture features in brain MR images for future developments in automatic denoising study. A total number of 39 image attributes were considered that are based on three categories: basic image statistics, GLCM, and Tamura texture features. A wide variety of 9344simulated T1-weighted MR images from the BrainWeb dataset were used to evaluate and test the image features. A t-test was applied to each individual image features computed in every image to evaluate the discrimination ability. It is observed that regardless of anatomical types of normal and MS there was no significant difference in the ranking of the features. For distinguishing between noise levels, the features of CON, SD, ASM, ENT, HOM, and DIS from

Table 4: T-test Results of MS Model Based on the P-Value: Noise Level

Thickness: 1mm	
p-value	Feature
<0.05	CON(0°, 45°, 90°, 135°), SD(x,0°, 45°, 90°, 135°), SD(y,0°, 45°, 90°, 135°),ASM(45°, 90°, 135°),ENT(0°,45°, 90°, 135°), CON, DIS(90°, 135°),HOM(45°)
< 0.1	DIS(0°, 45°), ASM(0°), HOM(0°, 90°, 135°),COR(0°,45°,90°,135°), ENT,SD,VAR
Thickness: 3mm	
p-value	Feature
<0.05	ENT(0°, 45°, 90°, 135°), SD(x,0°, 45°, 90°, 135°), SD(y,0°, 45°, 90°, 135°), CON(135°)
< 0.1	CON(0°, 45°, 90°), DIS(0°, 45°, 90°, 135°), HOM(45°, 90°, 135°), ASM(0°,45°, 90°, 135°), COR(0°, 45°, 90°, 135°), CON
Thickness: 5mm	
p-value	Feature
< 0.1	ASM(0°, 45°, 90°, 135°), SD(x,0°, 45°, 90°, 135°), SD(y,0°, 45°, 90°, 135°), DIS(0°, 45°, 90°, 135°), CON(0°, 45°, 90°, 135°), ENT(0°, 45°, 90°, 135°), COR(0°, 45°, 90°, 135°) , HOM(45°, 135°) , CON
Thickness: 7mm	
p-value	Feature
< 0.1	SD(x,0°, 45°, 90°, 135°),SD(y,0°, 45°, 90°, 135°), CON(0°, 45°, 90°, 135°), CON, HOM(45°, 135°), DIS(0°, 45°, 135°), ASM(0°, 45°, 90°, 135°), ENT(0°, 45°, 90°, 135°), COR(0°, 45°, 90°, 135°)
Thickness: 9mm	
p-value	Feature
< 0.1	CON, HOM(45°, 135°), SD(x,0°, 45°, 90°, 135°), SD(y,0°, 45°, 90°, 135°), CON(0°, 45°, 90°, 135°), ASM(0°, 45°, 90°), COR(0°, 45°, 90°) , DIS(0°, 45°, 135°)

the GLCM class performed best. For distinguishing between slice positions, the features of Mean and VAR from the basic statistics class and the feature of COA from the Tamura class performed best. Nevertheless, the order of significance in the texture features approximately varied in noise level, slice position as well as models in both normal and MS cases.

ACKNOWLEDGEMENT

This work was supported by the National Taiwan University under Grant No. NTU-CDP-103R7889.

REFERENCES

[1] Toga AW, "The laboratory of neuro imaging: what it is, why it is, and how it came to be," Medical Imaging, IEEE Transactions on 2002; 21: 1333-1343. http://dx.doi.org/10.1109/TMI.2002.806432

[2] Hashemi RH, Bradley WG, Lisanti CJ. MRI: the basics: LWW 2012.

[3] Westbrook C, Roth CK. MRI in Practice: Wiley-Blackwell 2011.

[4] Gudbjartsson H, Patz S. "The Rician distribution of noisy MRI data," Magnetic Resonance in Medicine, 1995; vol. 34: 910-914. http://dx.doi.org/10.1002/mrm.1910340618

[5] Macovski A. "Noise in MRI," Magnetic Resonance in Medicine 1996; vol. 36: 494-497. http://dx.doi.org/10.1002/mrm.1910360327

[6] Chang HH, Chiang MC, Sheu TWH, Huang H. "A contrast-enhanced trilateral filter for MR image denoising," in Biomedical Imaging: From Nano to Macro, 2011 IEEE International Symposium on, 2011; 1823-1826.

[7] Chang HH, Chu WC. "Restoration algorithm for image noise removal using double bilateral filtering," Journal of Electronic Imaging 2012; vol. 21: 023028-1-023028-13. http://dx.doi.org/10.1117/1.JEI.21.2.023028

[8] He L, Greenshields R. Ian, "A nonlocal maximum likelihood estimation method for Rician noise reduction in MR images," Medical Imaging, IEEE Transactions on 2009; vol. 28: 165-172.

[9] Tomasi C, Manduchi R. "Bilateral filtering for gray and color images," in Computer Vision, 1998. Sixth International Conference on, 1998; 839-846.

[10] Liu X, Tanaka M, Okutomi M. "Noise Level Estimation Using Weak Textured Patches of a Single Noisy Image," Image Processing (ICIP), 2012 19th IEEE International Conference on 2012; 665-668.

[11] Haralick RM, Shanmugam K, Dinstein IH. "Textural features for image classification," Systems, Man and Cybernetics, IEEE Transactions on 1973; 610-621.

[12] Howarth P, Rüger S. "Robust texture features for still-image retrieval," IEE Proceedings-Vision, Image and Signal Processing 2005; vol. 152: 868-874. http://dx.doi.org/10.1049/ip-vis:20045185

[13] Majtner T, Svoboda D. "Extension of tamura texture features for 3d fluorescence microscopy," in 3D Imaging, Modeling, Processing, Visualization and Transmission (3DIMPVT), 2012 Second International Conference on 2012; 301-307.

[14] Zong L, Ying L, Daxiang L. "A new texture feature extraction method for image retrieval," in Intelligent Control and Information Processing (ICICIP), 2013 Fourth International Conference on 2013; 482-486.

[15] Fisher RA, Genetiker S, Genetician S, Britain G, Généticien S. Statistical methods for research workers 1970; vol. 14: Oliver and Boyd Edinburgh.

[16] Student, "The probable error of a mean," Biometrika 1908; 1-25.

[17] Craparo RM. "Significance level," in Salkind, Neil J. Encyclopedia of Measurement and Statistics, ed 2007; 889-891.

[18] Chang HH, "Entropy-based trilateral filtering for noise removal in digital images," Image and Signal Processing (CISP), 2010 3rd International Congress on, vol. 2, pp. 673-677, 16-18 Oct. 2010 201.

Received on 11-03-2015 Accepted on 27-03-2015 Published on 29-04-2015

http://dx.doi.org/10.15379/2409-3394.2015.02.01.4